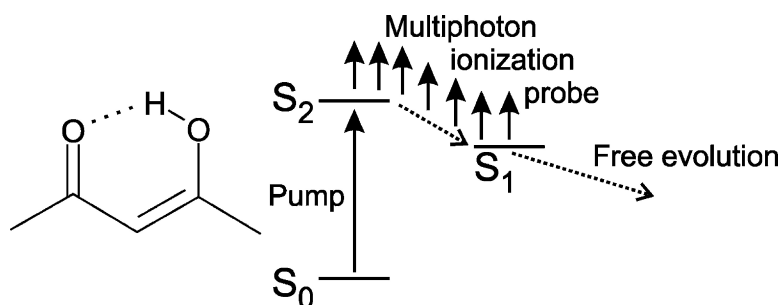## Article

Ultrafast Dynamics of Acetylacetone (2,4-Pentanedione) in the S State

Lionel Poisson, Pascale Roubin, Stphane Coussan, Benot Soep, and Jean-Michel Mestdagh

More About This Article

Additional resources and features associated with this article are available within the HTML version:

- Supporting Information
- Access to high resolution figures
- Links to articles and content related to this article
- Copyright permission to reproduce figures and/or text from this article

View the Full Text HTML

Ultrafast Dynamics of Acetylacetone (2,4-Pentanedione) in the S₂ State

Lionel Poisson,[†] Pascale Roubin,*,[‡] Stéphane Coussan,*,[‡] Benoît Soep,[†] and Jean-Michel Mestdagh[†]

Laboratoire Francis Perrin (CNRS-URA-2453), DSM/IRAMIS/Service des Photons, Atomes et Molécules, C.E.A. Saclay, F-91191 Gif-sur-Yvette cedex, France, and Laboratoire de Physique des Interactions Ioniques et Moléculaires, CNRS-UMR-6633, Université de Provence, Centre St-Jérôme, F-13397 Marseille cedex 20, France

Received May 2, 2007; E-mail: jean-michel.mestdagh@cea.fr

Abstract: The dynamics of the enolic form of acetylacetone (E-AcAc) was investigated using a femtosecond pump−probe experiment. The pump at 266 nm excited E-AcAc in the first bright state, $S_2(\pi\pi^*)$. The resulting dynamics was probed by multiphoton ionization at 800 nm. It was investigated for 80 ps on the $S_2(\pi\pi^*)$ and $S_1(n\pi^*)$ potential energy surfaces. An important step is the transfer from S_2 to S_1 that occurs with a time constant of 1.4 ± 0.2 ps. Before, the system had left the excitation region in 70 ± 10 fs. An intermediate step was identified when E-AcAc traveled on the S_2 surface. Likely, it corresponds to an accidental resonance in the detection scheme that is met along this path. More importantly, some clues are given that an intramolecular vibrational energy relaxation is observed, which transfers excess vibrational energy from the enolic group O−H to the other modes of the molecule. The present multistep evolution of excited E-AcAc probably also describes, at least qualitatively, the dynamics of other electronically excited β-diketones.

1. Introduction

Acetylacetone (full name 2,4-pentanedione) is a β-diketone where the keto−enol tautomerism is almost totally shifted toward the enolic form both in the gas phase[1,2] and isolated in cryogenic matrices.[3] Enolic acetylacetone (hereafter abbreviated as E-AcAc) has eight rotamers. The most stable is:[3]

(1)
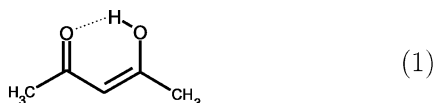
Its stability is due to the intramolecular H bond, shown as a dashed line in the scheme above. The central six-membered ring, closed by the intramolecular H bond, is a key structural property that E-AcAc shares with many molecules: a simpler molecule is malonaldehyde (propanedial), for which the two CH₃ groups are replaced by H atoms, and much more complex molecules are salicylic acid, biomolecules, or photochromic molecules. The H atom that closes the central ring of these molecules is in proper position to transfer from one O atom to the other. Hence, these molecules belong to an important class where an intramolecular H-atom transfer reaction, one of the most important reactions in chemistry,[4] can be turned on by electronic excitation.[5]

The two methyl groups in E-AcAc (as the H atoms in malonaldehyde) are symmetrically distributed about the central six-membered ring, making the product in the intramolecular H-atom transfer identical to the parent molecule. This process is very rapid and certainly affects the early dynamics of these molecules when excited electronically, but the full dynamics is considerably more complex than a simple H-atom transfer. Extensive experimental works on E-AcAc have identified various exit channels as dissociation,[6−8] isomerization to different rotamers,[3,9−12] and enol−keto tautomerization.[12]

Recent ab initio calculations have shown that the first strong electronic transition of E-AcAc corresponds to $S_2 \leftarrow S_0$.[11,13] It has a strong $\pi\pi^*$ character, whereas the $S_1 \leftarrow S_0$ excitation mainly corresponds to a $n\pi^*$ transition. The calculated equilibrium configuration in S_0 is that shown in eq 1 where the H

---

† C.E.A. Saclay.
‡ Université de Provence.

(1) Irving, R. J.; Wadso, I. *Acta Chem. Scand.* **1970**, *24*, 589−598.
(2) Temprado, M.; Roux, M. V.; Umnahanant, P.; Zhao, H.; Chickos, J. S. *J. Phys. Chem. B* **2005**, *109*, 12590−12595.
(3) Roubin, P.; Chiavassa, T.; Verlaque, P.; Pizzala, L.; Bodot, H. *Chem. Phys. Lett.* **1990**, *175*, 655−659.

(4) *Hydrogen-Transfer Reactions*; Hynes, J. T., Klinman, J. P., Limbach, H.-H., Schowen, R. L., Eds.; Wiley-VCH Verlag GmbH and Co.KG aA: Weinheim, Germany, 2007.
(5) Douhal, A.; Lahmani, F.; Zewail, A. H. *Chem. Phys.* **1996**, *207*, 477−498.
(6) Yoon, M. C.; Choi, Y. S.; Kim, S. K. *J. Chem. Phys.* **1999**, *110*, 11850−11855.
(7) Upadhyaya, H. P.; Kumar, A.; Naik, P. D. *J. Chem. Phys.* **2003**, *118*, 2590−2598.
(8) Xu, S.; Park, S. T.; Feenstra, J. S.; Srinivasan, R.; Zewail, A. H. *J. Phys. Chem. A* **2004**, *108*, 6650−6655.
(9) Chiavassa, T.; Verlaque, P.; Pizzala, L.; Allouche, A.; Roubin, P. *J. Phys. Chem.* **1993**, *97*, 5917−5925.
(10) Coussan, S.; Manca, C.; Ferro, Y.; Roubin, P. *Chem. Phys. Lett.* **2003**, *370*, 118−125.
(11) Coussan, S.; Ferro, Y.; Trivella, A.; Rajzmann, M.; Roubin, P.; Wieczorek, R.; Manca, C.; Piecuch, P.; Kowalski, K.; Wloch, M.; Kucharski, S. A.; Musia, M. *J. Phys. Chem. A* **2006**, *110*, 3920−3926.
(12) Nagashima, N.; Kudoh, S.; Takayanagi, M.; Nakata, M. *J. Phys. Chem. A* **2001**, *105*, 10832−10838.
(13) Chen, X. B.; Fang, W. H.; Phillips, D. L. *J. Phys. Chem. A* **2006**, *110*, 4434−4441.

atom "belongs" to only one O atom.[14] This is also the case in S_1.[13] In contrast, the S_2 state has the H atom at the same distance of the two O atoms.[7,13] Hence, the vertical excitation $S_2 \leftarrow S_0$ puts the H atom out-of-equilibrium on the S_2 surface and induces the intramolecular H-atom transfer mentioned above. Many theoretical works have addressed this question, taking various molecules as representative examples (see ref 15 for a review of older works and refs 13, 16, and 17 for most recent investigations).

It is well-known in the photochemistry of organic molecules that the reactive state is not the initially populated one. Ultrafast nonadiabatic energy transfers take place prior to the system reaching the reactive state.[18−20] Recent calculations indicate that E-AcAc also follows this rule.[13]

Zewail and co-workers documented the real-time dissociation dynamics of E-AcAc, following excitation to the $S_2(\pi\pi^*)$ state. The electron diffraction technique was used as a probe, indicating that the loss of OH was achieved with a time constant of 247 ± 34 ps.[8] This time was assigned to the lifetime of the $S_1(n\pi^*)$ state of E-AcAc, assuming that it decays through the intersystem crossing $T_1(\pi\pi^*) \leftarrow S_1(n\pi^*)$. According to this work, $S_1(n\pi^*)$ was populated from $S_2(\pi\pi^*)$ through an ultrafast nonadiabatic process that could not be resolved, apparently because the S_2 and S_0 states have geometries that can hardly be separated in the diffraction peaks.

The present work aims at experimentally exploring the ultrafast dynamics of E-AcAc in order to document the nonadiabatic transfer from $S_2(\pi\pi^*)$ to $S_1(n\pi^*)$, using the standard femtochemistry technique that associates time-resolved photoelectron spectroscopy[21] and velocity map imaging (VMI) of ions and electrons.[22]

2. Experimental Section

The experiment was carried out using the LUCA femtosecond laser at the Saclay Laser-matter Interaction Center (the SLIC facility), where the gas-phase E-AcAc molecule was excited with 266 nm pulses (the pump) and probed by ionization with 800 nm pulses. The experimental apparatus is described elsewhere.[20] The photoions and photoelectrons produced by the probe were analyzed both by an ion time-of-flight mass spectrometer (TOF-MS) and by a VMI device, the corresponding signals being monitored as a function of the delay between the pump and probe pulses.

The E-AcAc molecule was injected in two ways in the interaction region with the lasers, as a cold beam and as a room-temperature vapor. In the first case, the E-AcAc beam was prepared by supersonic expansion of a helium/E-AcAc mixture into vacuum through a pulsed valve operating at 20 Hz. Commercial acetylacetone from Aldrich, a liquid at room temperature, was used with no further purification. The helium/E-AcAc mixture was achieved by putting liquid acetylacetone in a small chamber on the helium foreline. The vapor pressure of acetylacetone in this chamber was great enough for helium to be seeded by gaseous acetylacetone evaporating from the liquid. In the second case, E-AcAc was injected as a room-temperature vapor directly into the ionization region of the VMI through a needle. According to ref 1,
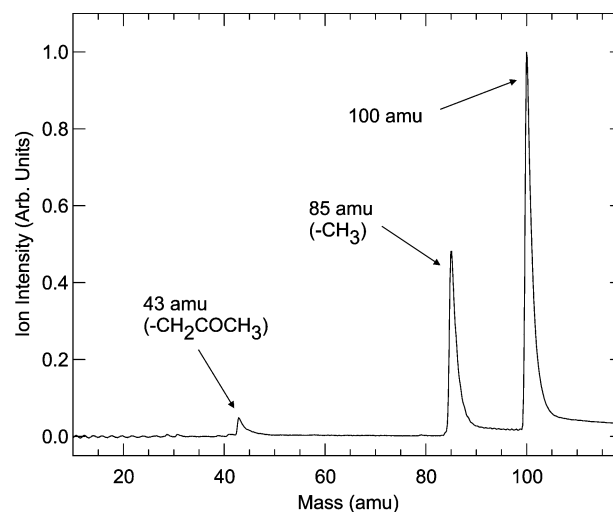
(14) Srinivasan, R.; Feenstra, J. S.; Park, S. T.; Xu, S.; Zewail, A. H. *J. Am. Chem. Soc.* **2004**, *126*, 2266−2267.
(15) Scheiner, S. *J. Phys. Chem. A* **2000**, *104*, 5898−5909.
(16) Aquino, A. J. A.; Lischka, H.; Hättig, C. *J. Phys. Chem. A* **2005**, *109*, 3201−3208.
(17) Coe, J. D.; Martinez, T. J. *J. Phys. Chem. A* **2006**, *110*, 618−630.
(18) Mestdagh, J. M.; Visticot, J. P.; Elhanine, M.; Soep, B. *J. Chem. Phys.* **2000**, *113*, 237−248.
(19) Gloaguen, E.; Mestdagh, J. M.; Poisson, L.; Lepetit, F.; Visticot, J. P.; Soep, B.; Coroiu, M.; Eppink, A.; Parker, D. H. *J. Am. Chem. Soc.* **2005**, *127*, 16529−16534.
(20) Poisson, L.; Raffael, K. D.; Soep, B.; Mestdagh, J. M.; Buntinx, G. *J. Am. Chem. Soc.* **2006**, *128*, 3169−3178.
(21) Stolow, A.; Bragg, A. E.; Neumark, D. M. *Chem. Rev.* **2004**, *104*, 1719−1757.
(22) Eppink, A.; Parker, D. H. *Rev. Sci. Instrum.* **1997**, *68*, 3477−3484.

Figure 1. Mass spectrum obtained using the TOF-MS instrument and the pump and probe pulses set at zero delay.

93.3% of gaseous acetylacetone at room temperature is under the enolic form E-AcAc. Since molecules are cooled down when carried into a supersonic expansion, the fraction of E-AcAc present in the beam experiment was certainly greater than 93.3%. Hence, whatever the injection method, E-AcAc was the dominant species in the experiments reported below. No significant differences were observed in the measured signal whether E-AcAc was injected as a beam or as a room-temperature vapor, except for the signal-to-noise ratio, which was higher in the latter case. Except when stated explicitly, the results below were taken using the direct injection method.

The pump and probe laser beams were approximately collinear and overlapped at the crossing point with the molecular beam (or at the output of the needle in the direct injection method). The probe ionized electronically excited E-AcAc molecules. To detect the resulting charged particles, the overlap region between the lasers was located in the ionization region shared by the TOF-MS and VMI spectrometers. The latter was used for mapping the kinetic energy and the angular distributions of the electrons resulting from the ionization by the probe laser.[22]

The femtosecond pump and probe pulses were generated from a laser chain associating a Ti:Sapphire oscillator and an amplifier. The full system was operated at a 20 Hz repetition rate, a 800 nm wavelength, and a ca. 50 fs pulse duration. A fraction of the output was tripled and provided the pump pulse at 266 nm. The residual output served to probe the molecule by multiphoton ionization at 800 nm as performed by Fuss and co-workers.[23] The probe laser beam was passed through a delay line that allowed us to control the delay between the pump and the probe laser pulses. The power density of the laser light was adjusted by modifying the focusing of each laser beam in order to optimize the pump−probe contrast of the signals. This typically corresponded to a power density of 2×10^{11} W·cm^{-2} for the pump, whereas either a 5×10^{11} W·cm^{-2} (hereafter referred to as *soft focusing*) or a 1×10^{12} W·cm^{-2} (*mild focusing*) power density was used for the probe. Both operating conditions corresponded to a much lower power density than that used by Fuss and co-workers, 1×10^{13} W·cm^{-2}.[23]

The cross correlation between the pump and probe lasers measured in the interaction region with the molecular beam was ca. 80 fs. In the experiments reported below, the polarizations of the lasers were both horizontal, the extraction direction of the electrons being vertical.

3. Results

3.1. Recording Ions. Figure 1 displays the mass spectrum obtained with the TOF-MS instrument. E-AcAc was injected through the molecular beam, and the pump and probe lasers were set at zero delay. Three peaks appear at 100, 85, and

(23) Fuss, W.; Schmid, W. E.; Trushin, S. A. *J. Am. Chem. Soc.* **2001**, *123*, 7101−7108.
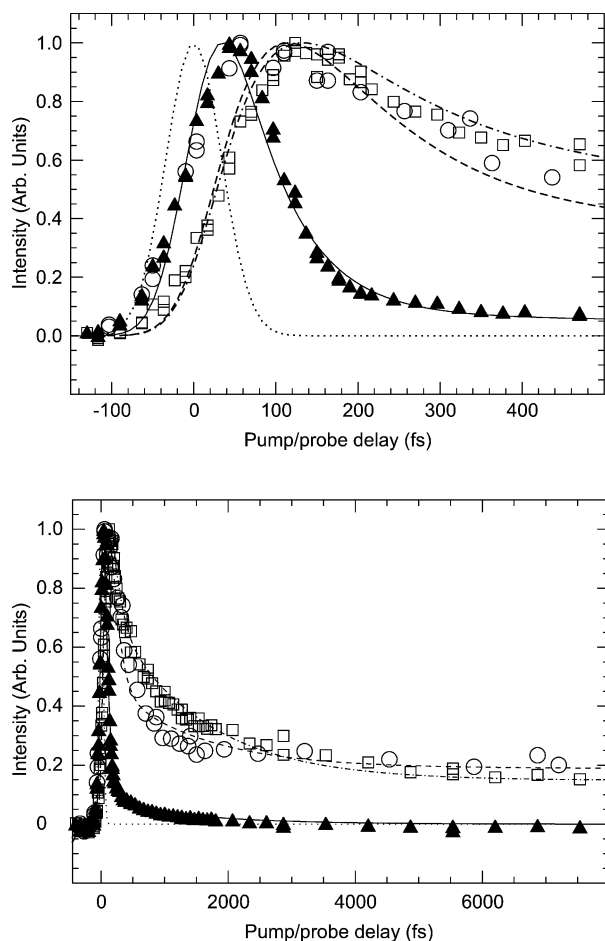
Figure 2. Ion signals recorded at masses 100 amu (triangles and solid line curve), 85 amu (open squares and dotted-dashed curve), and 43 amu (open circles and dashed curve) as a function of the pump/probe delay up to 500 fs (top figure) and 8 ps (bottom figure). The probe laser was operated under the mild focusing regime. The curves running through the experimental points are fits obtained using the parameters given in Table 2 and the kinetic model described in the text. The dotted curve shows the cross-correlation function of the two lasers.

43 amu. These peaks are also the main peaks observed in the electron impact ionization of gaseous acetylacetone.[24] The peak at 100 amu corresponds to the E-AcAc molecular ion. When internally hot, this ion can lose a CH_3 group, thus giving the peak at 85 amu. The peak at 43 amu corresponds to CH_3CO^+: it results from the fragmentation of quite hot E-AcAc ions, following a complex structural rearrangement.[25]

The dynamics of electronically excited E-AcAc was explored by recording the ion signals at masses 100, 85, and 43 amu as a function of the pump–probe delay, up to 80 ps for both the soft and mild focusing of the probe laser (see Section 2). The two panels in Figure 2 show the results taken with the mild laser focusing, up to 500 fs and 8 ps delay between the pump and the probe laser. A plateau is visible at long delay for the masses 43 and 85 amu. It was followed up to 80 ps and is slowly decaying. The corresponding results are not shown here. The experiments performed with the soft laser focusing are reported in Figure 3. No plateau is observed in this case.
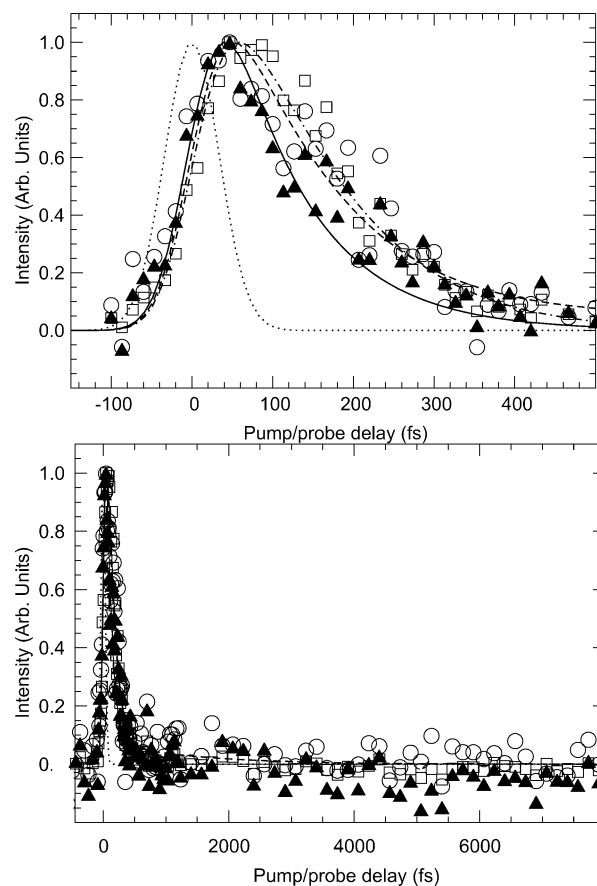
(24) Stein, S. NIST Mass Spectral Data Center. In *NIST Chemistry WebBook*, *NIST Standard Reference Database*; Mallard, W. G., Linstrom, P. J., Eds.; National Institute of Standards and Technology: Gaithersburg, MD, 2005; Vol. 69. http://webbook.nist.gov.

(25) Westmore, J. B.; Buchannon, W. D.; Plaggenborg, L.; Wenclawiak, B. W. *J. Am. Soc. Mass Spectrom.* **1998**, *9*, 29–34.

Figure 3. Same caption as in Figure 2, but the probe laser was operated under the soft focusing regime.

3.2. Recording Electrons. Electron images were taken using the VMI device, for various delays between the pump and the probe laser pulses. As above for the ions, experiments were performed with both the soft and mild focusing regimes of the lasers.

A raw electron image provided by the VMI device is a two-dimensional (2D) projection of the actual three-dimensional (3D) electron distribution. A cut through the 3D distribution is reconstructed numerically from the 2D projection by taking advantage of the cylindrical symmetry of the 3D distribution about the common polarization direction of the lasers. This was achieved using the p-BASEX algorithm.[26] A reconstructed image is shown in Figure 4. It documents both the kinetic energy E (square of the radius in the figure) and the ejection angle θ of the electrons with respect to the laser polarization (vertical in the figure).[22] To extract meaningful information from the set of images that was taken, each image was fitted in two steps: first the angular distribution, then the energy distribution.

The angular distribution of the electrons is conveniently described by the expression

$$\alpha(E, t)[1 + \beta_2(E, t)P_2(\cos \theta) + \beta_4(E, t)P_4(\cos \theta) + \beta_6(E, t)P_6(\cos \theta)] \quad (2)$$

where t is the delay between the pump and the probe pulses, E is the energy of the electrons, θ is their direction with respect to the laser polarization, and $P_{2,4,6}(\cos \theta)$ Legendre polynomials describing the anisotropy of the electron distribution. $\alpha(E, t)$

(26) Garcia, G. A.; Nahon, L.; Powis, I. *Rev. Sci. Instrum.* **2004**, *75*, 4989–4996.
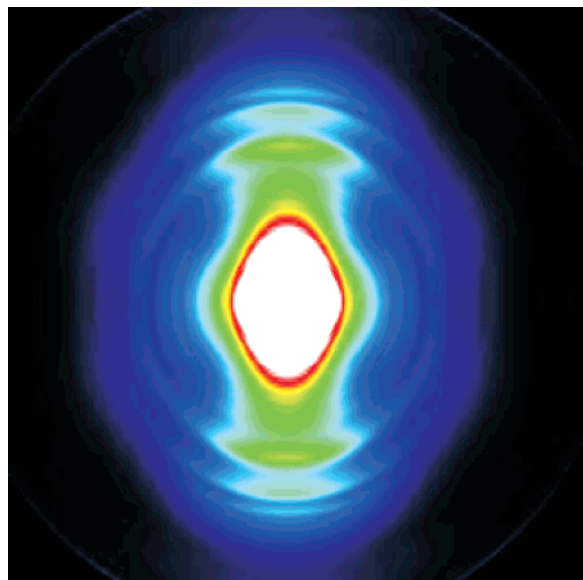
Figure 4. Electron image taken using VMI after reconstruction by the p-BASEX-algorithm (see the text). The probe laser was operated under the mild focusing regime.
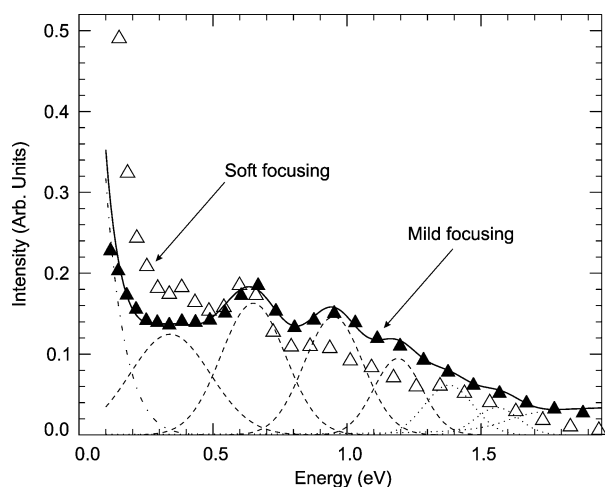

Figure 5. Electron spectra extracted from the electron images after summation over all the pump/probe delays. The full and open triangles refer to experiments under the mild and soft focusing regimes, respectively. The spectra are normalized with the same intensity at 0.65 eV. The solid line curve is a fit to the full triangle spectrum. It is obtained as a superposition of contributions marked as dotted-dashed, dashed, and dotted curves according to eq 3−5 and Table 1.

and $\beta_{2,4,6}(E, t)$ are the numerical functions used to fit the images. As we shall see later, the probe process is multiphotonic and the full pump−probe sequence may involve up to five photons. Hence, anisotropy terms up to the Legendre polynomial P_{10} could be expected. Nevertheless, the fit of the image necessitated anisotropy terms up to P_6 only, as stated in eq 2.

At this point, the full description of the images is provided by the four numerical functions $\alpha(E, t)$ and $\alpha(E, t) \times \beta_{2,4,6}(E, t)$. Each could be represented as a set of 3D plots showing these quantities as a function of E and t. However, we found it more convenient to solve the dependence of these quantities upon E as the superposition of several contributions corresponding to the emission of electrons of different energies. Such a superposition is especially apparent in Figure 5 which shows electron spectra obtained by integrating the function α over the entire range of delays explored experimentally. The open and full triangles of the figure refer to the soft and mild focusing of the

Table 1. Parameters Defining the Functions 3−5 Used to Fit the Electron Spectra, Given in eV

	s_0						
	0.14						
E_1	s_1	E_2	s_2	E_3	s_3	E_4	s_4
0.34 ± 0.01	0.15	0.65 ± 0.02	0.12	0.95 ± 0.03	0.11	1.19 ± 0.04	0.09
E_5	s_5	E_6	s_6	E_7	s_7		
1.38	0.09	1.56	0.08	1.60	0.1		

laser, respectively. The two spectra are normalized on the peak at $E = 0.65$ eV. They will be discussed fully in Section 5. Only the full triangle spectrum is considered here. It can be decomposed as an intense contribution at low energy plus a series of weakly structured contributions above 0.3 eV that become structureless above 1.2 eV. The low-energy contribution is adequately fitted by the expression

$$\frac{1}{E} \exp\left(-\frac{E^2}{2s_0{}^2}\right) \tag{3}$$

where s_0 reflects the width of the distribution. The other contributions are conveniently fitted by a series of six Gaussian functions ($i = 1-6$)

$$\exp\left(-\frac{(E - E_i)^2}{2s_i{}^2}\right) \tag{4}$$

plus the step function

$$\frac{\pi}{2} + \arctan\left(\frac{E - E_7}{s_7}\right) \tag{5}$$

which accounts for the high-energy limit of the spectrum. The E_i and s_i parameters that define the energy centering and width of these functions are given in Table 1. The location of the four first Gaussian functions is well-defined by the fit, and error ranges are provided for them in Table 1. Note that the two Gaussian functions centered at 1.38 and 1.56 eV and the step function simply serve as basis functions to allow the fitting of the structureless part of the spectrum above 1.2 eV.

Figure 6 shows electron spectra as the delay between the pump and probe pulses is changed. The curves shown in the figure were obtained by integrating the function $\alpha(E, t)$ over various ranges of delays as indicated in the figure caption. The top and bottom panels correspond to the soft and mild laser focusing regimes, respectively. In each panel the curves are normalized with the same intensity over the range of 0.10− 0.15 eV. Importantly, the energy location of the structures observed in the spectra does not change when the delay is changed. Only their relative intensity changes. This justifies the choice made here of fitting the electron spectra at each delay by adjusting the relative importance of the contributions described by the functions 3−5 without changing the parameter values given in Table 1. The individual contributions to the isotropic part $\alpha(E, t)$ of the electron signal are plotted as a function of the pump−probe delay in Figures 7 and 8, for the soft and mild laser focusing regimes, respectively.

In the same way, the individual contributions to the $\beta_{2,4,6}(E, t)$ functions describing the anisotropy of the electron signal were extracted from the experimental data and plotted as a function of the pump−probe delay. With the soft focusing arrangement, only the anisotropy term $\beta_2(E, t)$ could be observed. The
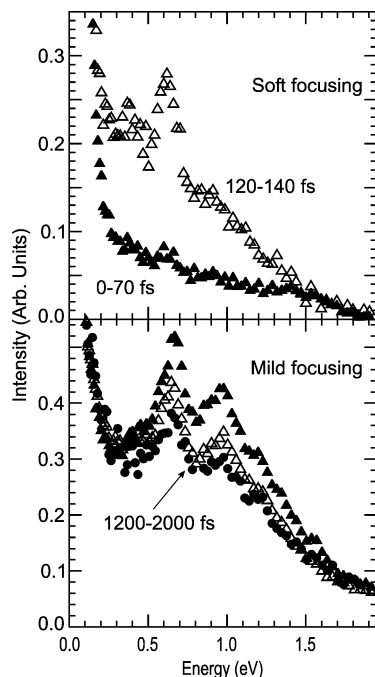
Figure 6. Electron spectra extracted from the electron images after summation over various ranges the pump/probe delays. The top (respectively, bottom) panel reports the experiment performed under the soft (respectively, mild) focusing regime. In each panel, the full and open triangles refer to the range of delays 0−70 fs and 120−400 fs, respectively, and the full circles in the bottom panel refer to the range of 1200−2000 fs.
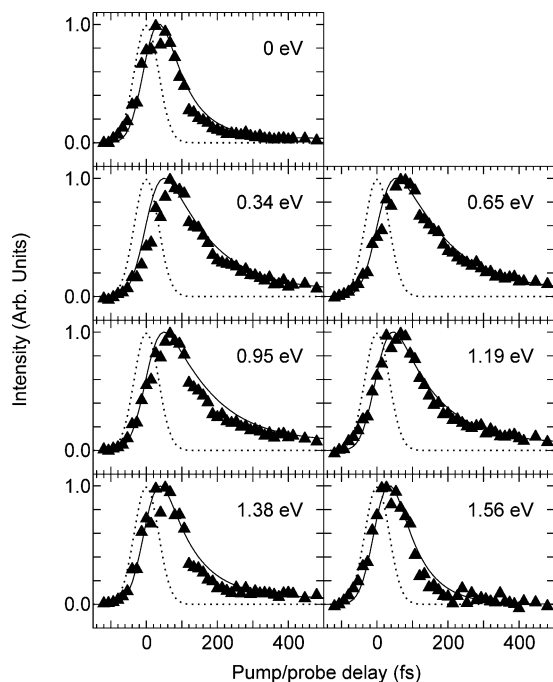

Figure 7. Contributions described by eqs 3 and 4 to the isotropic part $\alpha(E)$ of the electron signal as a function of the pump/probe delay. The curves are best fits to the data points. The data were taken under the soft focusing regime. The dotted curves are the cross-correlation functions of the lasers.
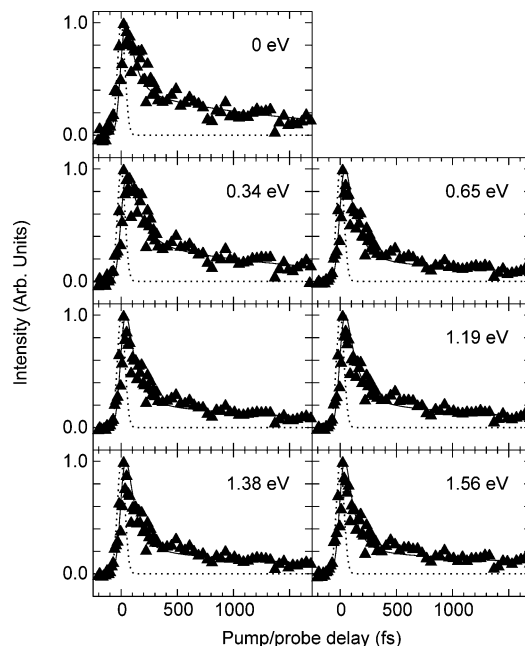

Figure 8. Same caption as in Figure 7, but for the isotropic part $\alpha(E, t)$ and data taken under the mild focusing regime.
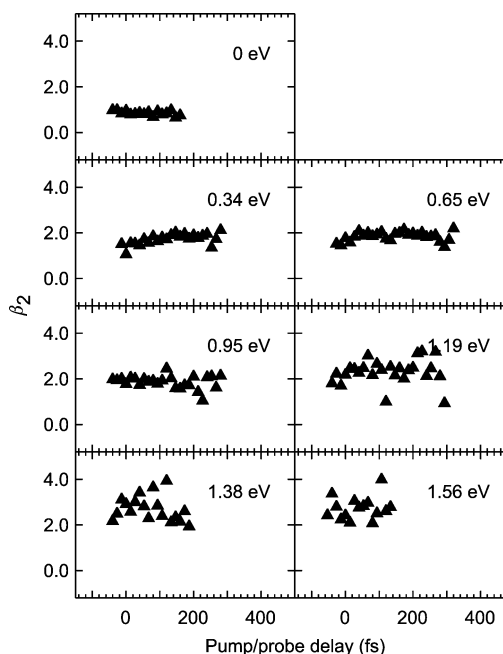

Figure 9. Contributions described by the eqs 3 and 4 to the anisotropic part $\beta_2(E)$ of the electron signal as a function of the pump/probe delay. The data were taken under the soft focusing regime.

corresponding results are shown in Figure 9 at delays where the signal in Figure 7 is more than 0.2 times the maximal signal, i.e., large enough for the β_2 determination to be fairly accurate. No dependence of β_2 is observed with the pump−probe delay.

Depending on the class of electrons that is considered, the value of $\beta_2(E, t)$ ranges from 1.00 ± 0.05 for the electrons of zero energy to 2.0 ± 0.1 for the electrons of 0.34, 0.65, and 0.95 eV, up to 2.8 ± 0.1 for the electrons of largest energy. The latter observation, which is apparently surprising, simply reflects that the ionization process is multiphotonic. Hence, $\beta_2(E, t)$ is not restricted to the range $[-1, 2]$ as expected in a one-photon process. This will be discussed later. $\beta_{2,4,6}(E, t)$ functions could be measured with the mild focusing arrangement. The $\beta_6(E, t)$ contribution is shown in Figure 10. It varies with both the energy of the electrons and the pump−probe delay.
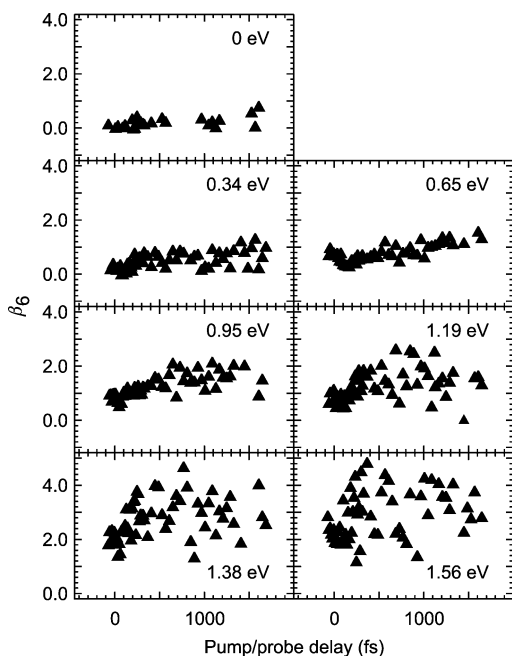
Figure 10. Same caption as in Figure 9, but for the anisotropic part $\beta_6(E, t)$ and data taken under the mild focusing regime.

4. Analysis of the Time Dependencies

The time dependencies of the signals that appear in Figures 2 and 3 and 7 and 8 have a multiexponential character. The simplest linear kinetic model that was appropriate to fit all these data is a sequential decay involving four transients of E-AcAc

$$A \xrightarrow{\tau_A} B \xrightarrow{\tau_B} C \xrightarrow{\tau_C} D \qquad (6)$$

where τ_A, τ_B, and τ_C represent the decay times from one transient to the other. In the discussion, the four transients A, B, C, and D will be corresponded to different electronic states or geometrical conformations of the electronically excited E-AcAc. Upon ionization, each transient produces the observed species (ions of masses 100, 85, or 43 amu and electrons of various energies) with yields σ_A, σ_B, σ_C, and σ_D that include the ionization cross section of the transient under consideration and the branching ratio to the specific species that is observed.

The expressions describing the time evolution of the populations of transients A–D in the kinetic model eq 6 are given in ref 20. They are used to fit the data of Figures 2 and 3 and 7 and 8 after numerical convolution by the cross-correlation function of the pump and probe laser pulses (80 fs). The fit parameters τ_A, τ_B, and τ_C represent intrinsic properties of E-AcAc. Hence, the same set of values is used to fit all the experimental data. In contrast, the detection efficiencies σ_A, σ_B, σ_C, and σ_D contain properties of the detection scheme (branching ratio to the observed species and multiphotonic character of the ionization). Hence, the parameters σ_A, σ_B, σ_C, and σ_D are adjusted for each curve in Figures 2 and 3 and 7 and 8. The best-fit parameters are given in Table 2. Since no absolute signal is detected in the present work, the detection efficiencies must be normalized. The expression $\sigma_A + \sigma_B + \sigma_C + \sigma_D = 1$ was chosen for the ions, and the expression $\sigma_A = 1$ was chosen for the electrons in Table 2.

When considering the signal at mass 43 amu at short delays in the top panel of Figure 2 (open circles), a very odd behavior

Table 2. Best-Fit Parameters Used in the Kinetic Model Expressed by Eq 6[a]

Figure	curve	τ_A (fs) 70 ± 10 σ_A	τ_B (fs) 100 ± 20 σ_B	τ_C (fs) 1400 ± 200 σ_C	σ_D
2 (MF)	100 amu	0.97	<0.01	0.034	<0.01
	85 amu	<0.01	0.69	0.26	0.054
	43 amu	<0.01	0.76	0.17	0.069
3 (SF)	100 amu	0.77	0.23	<0.01	<0.01
	85 amu	0.43	0.57	<0.01	<0.01
	43 amu	0.54	0.43	0.027	<0.01
7 (SF)	0 eV	1.0	0.01	0.02	<0.01
	0.34 eV	1.0	0.75	0.05	<0.01
	0.65 eV	1.0	1.00	0.07	<0.01
	0.95 eV	1.0	0.75	0.07	<0.01
	1.19 eV	1.0	0.50	0.05	<0.01
	1.38 eV	1.0	0.17	0.03	<0.01
	1.56 eV	1.0	<0.01	<0.01	<0.01
8 (MF)	0 eV	1.0	0.29	0.21	0.01
	0.34 eV	1.0	0.72	0.26	0.02
	0.65 eV	1.0	0.33	0.12	0.02
	0.95 eV	1.0	0.26	0.12	0.02
	1.19 eV	1.0	0.40	0.14	0.02
	1.38 eV	1.0	0.26	0.12	0.02
	1.56 eV	1.0	0.19	0.11	0.03

[a] The indications SF and MF in the first column refer to the soft and mild focusing regimes of the probe laser, respectively.

is observed that is not accounted for by the kinetic model (dashed curve). This signal (open circles) rises as the signal at mass 100 (full triangles) and decays as the signal at mass 85 amu (open squares). Such a behavior is impossible to fit with the sequential kinetic model of eq 6. The dashed curve in Figure 2 does not attempt to fit the rising part of the ion signal at mass 43 amu. Only the decay is fitted. In contrast, this odd behavior does not appear in Figure 3, and the full signal at mass 43 amu is adequately fitted by the kinetic model. The difference between the two experiments is the power density of the probe laser, which is higher in Figure 2 and which is likely to induce multiphotonic processes. The odd behavior of the signal at mass 43 amu appears within the cross correlation of the pump and the probe. We infer that it is related to a multiphotonic excitation/ionization process, far above the ionization threshold of E-AcAc, where both pump and probe photons are involved, that would produce either ions of mass 100 amu in a direct ionization process or very hot ions of mass 85 amu in an autoionization process. The latter ions, because of their large internal energy, are expected to fragment with a 100% probability as CH_3CO^+ ions (mass 43 amu). Mass spectrometry measurements of acetylacetone have shown indeed that the formation of the CH_3CO^+ fragment ion is subsequent to the formation of the 85^+ amu ion (loss of CH_3) when enough internal energy is present.[25]

5. Discussion

5.1. Energetics. The energetics of the E-AcAc system is given in Figure 11. It is constructed as stated in the figure caption. Whereas the excitation to the S_2 state is a single-photon process, the ionization probe is necessarily a multiphoton process.

From Figure 11, the vertical excitation energy of the S_2 state and the energy of three probe photons put E-AcAc between the adiabatic and vertical ionization energies from the ground state. Detecting E-AcAc while the molecule is in the Franck–Condon region of excitation is possible in a three-photon autoionization process, and the energy of the corresponding
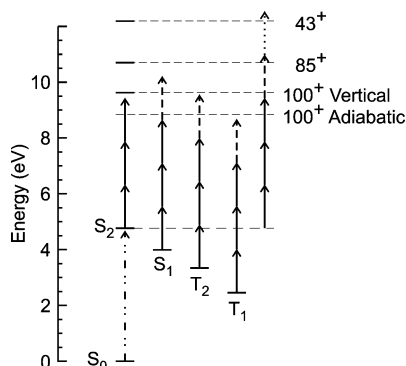
Figure 11. Energetics of E-AcAc: neutral, ion, and fragment ions. Energies are referred to the ground state of the chelated isomer shown in eq 1. The S_2 state is placed at its vertical excitation energy from the ground state.[11] The other excited states S_1, T_2, and T_1 are placed at their equilibrium energies as calculated in ref 13. The ion energetics are provided by mass spectrometric measurements[25] and the NIST/EPA/NIH mass spectral data base.[24] The vertical ionization energy corresponds to ionization from ground state E-AcAc. The arrows represent the energies of the pump (dot-dot dashed) and probe photons.

electrons will be fairly small. The absorption of a fourth probe photon would put the system above the vertical ionization energy, opening a direct ionization process. Electrons of almost 1.5 eV energy are expected in this case. Note that many molecular Rydberg levels are present between S_2 and the vertical ionization limit, and the efficiency of the multiphotonic ionization can be enhanced by intermediate resonances.

Figure 11 shows that the ionization of S_1 from its equilibrium geometry is energetically allowed with four photons or more. In fact, a four-photon ionization of this state is quite unlikely for two reasons that both make the actual ionization energy of S_1 higher than that expected from the figure. The vertical ionization energy indicated in the figure is from the ground state of E-AcAc, whereas the four-photon ionization process operates from the S_1 state, whose geometry differs from that of the ground state. No calculation is available on the E-AcAc cation, but one is available for malonaldehyde where the potential energies of neutral and cationic malonaldehyde are considered along the H-atom transfer coordinate.[27] It appears that the vertical ionization of the S_1 state requires 0.6 eV more energy than that expected when considering the vertical ionization energy from ground-state malonaldehyde (see Figure 4 in ref 27). Considering that the same situation prevails with E-AcAc, this is a first reason why the actual ionization energy could be larger than that suggested in Figure 11. The second reason refers to Koopman's theorem. In a direct vertical ionization of S_1-($n\pi^*$), the excited electronic configuration n^{-1} of the ion is formed, whereas ionization from $S_0(\pi^2)$ or $S_2(\pi\pi^*)$ would lead to the ground-state configuration π^{-1}.[27] Again the actual ionization energy is larger than expected. Hence, a five-photon process is more likely than a four-photon process for ionizing S_1 from its equilibrium geometry.

5.2. Assignment of Transient D to the S_1 State. Let us first compare the bottom panels of Figures 2 and 3. A plateau appears in the signals recorded at masses 43 and 85 amu at long time delays in Figure 2 whereas no such plateau exists at mass 100 amu. Moreover no plateau is observed within experimental uncertainties in Figure 3. Similarly, a plateau can be recognized in the electron data reported under the mild focusing regime in

Figure 8 whereas no plateau appears in Figure 7 under the soft focusing regime.

According to the kinetic model, observing a plateau at long time delays would correspond to the detection of transient D. This is actually reflected in Table 2 where the fit parameter σ_D has a nonzero value for the experimental observation mentioned above when fitting ion signals at 43 and 85 amu in Figure 2 and electron signals in Figure 8. These experiments were performed under the mild focusing regime of the lasers. In contrast, σ_D is equal to zero, within the experimental uncertainty, in the experiments performed with the soft focusing regime of the lasers. Hence, transient D is likely observed through an ionization process of larger multiphotonic character that forms the E-AcAc ion with enough internal energy to fragment.

The discussion above comparing the multiphotonic character of the S_2 and S_1 ionizations suggests that transient D could correspond to the detection of the S_1 state in a five-photon ionization process. Since this observation occurs at long pump–probe delays, a broadening of the absorption bands is expected, due to the energy randomization in the detected state. Hence, a larger number of intermediate resonances can be found from these broader absorption bands, resulting in an enhanced efficiency of the multiphotonic ionization.

Of course, similar considerations could be made for the even more multiphotonic detection of the T_2 and T_1 states of E-AcAc, hence leading to the assignment of transient D to one of these states. Nevertheless, we do not consider that this assignment is correct, because it is not consistent with the previous observations of Zewail and co-workers on the same system.[8] Following the electronic excitation of E-AcAc to the $S_2(\pi\pi^*)$ state, these authors observed a long-lived intermediate, which decays with a time constant of 247 ± 34 ps. It was assigned to the $S_1(n\pi^*)$ state slowly decaying through the intersystem crossing $T_1 \leftarrow S_1$. In the present work, the plateau was followed over 80 ps and is slowly decaying, consistently with the time constant of 247 ± 34 ps given in ref 8.

Consequently, the present transient D of excited E-AcAc is assigned to the slowly decaying state $S_1(n\pi^*)$ identified in ref 8.

5.3. Assignment of Transient C to a Region of Strong Coupling between the S_2 and S_1 States. From the calculations by Chen et al., no electronic state exists between $S_2(\pi\pi^*)$, which was populated initially by the pump laser and $S_1(n\pi^*)$, which has just been assigned to transient D.[13] Hence, we infer that the transients A, B, and C of excited E-AcAc that appear in the kinetic model of eq 6 correspond to various steps in the evolution of the wavepacket through the $S_2(\pi\pi^*)$ surface. In particular, transient C, which is met prior to the system transfers to transient D, likely corresponds to a region of strong coupling between $S_2(\pi\pi^*)$ and $S_1(n\pi^*)$. The existence of such a region has been considered in the calculation of ref 13. It might be a conical intersection by analogy with the situation in malonaldehyde, for which extensive potential calculations are available.[17] Accordingly, the time constant $\tau_C = 1.4 \pm 0.2$ ps is assigned to the timescale for the full transfer of the wavepacket from $S_2(\pi\pi^*)$ to $S_1(n\pi^*)$.

A fairly slow $S_2(\pi\pi^*) \rightarrow S_1(n\pi^*)$ transfer has been reported on a similar system of *o*-hydroxybenzaldehyde by Stolow and

(27) Sobolewski, A. L.; Domcke, W. *Chem. Phys. Lett.* **1999**, *310*, 548−552.

co-workers.[28] This molecule is a β-diketone and, as acetylacetone, it is stable as an enol in the gas phase. As E-AcAc, its first excited state S_1 also has a $n\pi^*$ character whereas the first bright state S_2 has a $\pi\pi^*$ character (note that the latter state is called S_1 in ref 28 probably because it is the first bright state. However, it seems more appropriate to call it S_2). Since the substituents attached to the central ring in enolic o-hydroxybenzaldehyde are not identical, the H-atom transfer occurs between two unsymmetrical minima of the $S_2(\pi\pi^*)$ potential energy surface. They are separated by a very shallow barrier (or no barrier). This makes the H-atom transfer within S_2 extremely rapid, and only an upper limit of its time constant, 50 fs, could be given in ref 28. In contrast, the relaxation time of the S_2 population could be measured. It ranges between 1.6 and 5.9 ps depending on the excess energy that was deposited in the S_2 state by the pump laser. These values are on the same order of magnitude as the 1.4 ± 0.2 ps lifetime found in the present work for the $S_2(\pi\pi^*)$ state of E-AcAc. The reason invoked in ref 28 to account for the lifetime of the $S_2(\pi\pi^*)$ of enolic o-hydroxybenzaldehyde is similar to that presently discussed for E-AcAc: the coupling between the $S_2(\pi\pi^*)$ state and a closely lying $n\pi^*$ state. Importantly, Stolow and co-workers[28] have explored another enolic β-diketone, 1-hydroxy-2-acetonaphtone, where the enolic ring is conjugated with a benzene ring.[28] A transition of $n\pi^*$ character is fairly localized and should not be influenced dramatically by the nature of the substituents about the central ring of enolic β-diketones. In contrast, the $\pi\pi^*$ excitation energy is lowered significantly by the conjugation. Therefore, the excited $\pi\pi^*$ state of 1-hydroxy-2-acetonaphtone has a lower energy than the $n\pi^*$ state. In this case, the lifetime of the $\pi\pi^*$ state is controlled by an internal conversion to the ground state S_0 and it is very long, 33 ps.[28]

Transient C is thus assigned to the region of strong coupling between $S_2(\pi\pi^*)$ and $S_1(n\pi^*)$, presumably a conical intersection, close to the equilibrium geometry of the S_2 surface.

5.4. Assignment of Transient A to the "Franck−Condon" Region of the Excitation. Section 5.1 suggests that a three-photon autoionization process allows one to detect the wavepacket formed in the S_2 state by the pump laser, as it is still in the Franck−Condon region of excitation. This ionization process should produce photoelectrons of fairly small energy, as those observed in the left-hand side of the photoelectron spectra of Figure 5 (electrons labeled with "0 eV" in Figures 7−10, which are described by eq 3). To observe such electrons, it is better to limit higher multiphotonic processes, and the soft focusing regime is more appropriate. The corresponding fit parameters provided in Table 2 show that these electrons reflect transient A almost exclusively ($\sigma_A = 0.97$ for the 0 eV electrons of Figure 7). These electrons also have the smallest anisotropy, in agreement with their origin, an autoionization. Nevertheless, the nonzero value of the anisotropy parameter β_2 in Figure 9 is surprising. A large part of its origin is probably an experimental artifact, which is especially apparent for the electrons of low energy.

The discussion in Section 5.1 indicates also that a direct four-photon ionization process producing electrons of ca. 1.5 eV allows one to detect the wavepacket in the same region. The fit parameters of the 1.56 eV electrons of Figure 7 (see Table 2

where $\sigma_A = 1.00$ for these electrons) confirm this expectation. Not surprisingly, the corresponding β_2 parameter (see Figure 9) is large, almost 3, in agreement with a photoionization process where two or more photons of a parallel excitation fix the anisotropy of the electron distribution.

We thus assign transient A to a region of the "Franck−Condon" region when exciting $S_2(\pi\pi^*)$ from S_0 surface with the pump laser. The quotation marks stress the discussion below which suggests that this region is actually the Franck−Condon region except for the H-atom coordinates. The time spent by the wavepacket in this region is $\tau_A = 70 \pm 10$ fs. The geometry of E-AcAc in this region corresponds to a vertical excitation and must be close to that shown in eq 1 where the H atom is closer to one of the O atoms. As said in the Introduction, this places the H atom off the equilibrium position of the S_2 state where the H atom is shared equally by the two O atoms. Given the lightness of the H atom, the deformation of E-AcAc that starts first in the S_2 state is a transfer of the H atom toward the other O aom, across the equilibrium position. The work of Stolow and co-workers on o-hydroxybenzaldehyde has shown that the H-atom transfer is achieved in less than 50 fs.[28] This is likely to be the case in E-AcAc also. Therefore, the time constant of $\tau_A = 70 \pm 10$ fs found for the decay of transient A in Table 2, which is longer than 50 fs, certainly reflects that deformation other than the sole H-atom transfer moves the molecule off the excitation region. Out-of-plane deformations of the central ring probably play a role in E-AcAc which does not appear in the more rigid o-hydroxybenzaldehyde molecule. Such deformations have been brought to light by the theoretical work of Martinez and Coe on the even less rigid molecule, malonaldehyde.[17] Note that the deformations which accompany the decay of transient A constitute the initial step where part of the electronic energy provided by the pump laser is redistributed over the vibrational modes of the molecule.

5.5. Assignment of Transient B to an Ionization Resonance. Since transient A is assigned to a region overlapping the excitation region by the pump laser, we have to assume that transient B reflects the detection of E-AcAc in the S_2 state, on its way between the excitation region (transient A) and the region of strong coupling between S_2 and S_1 (transient C). Accordingly, transient B would be populated from transient A with a time constant $\tau_A = 70 \pm 10$ fs whereas it decays with the time constant $\tau_B = 100 \pm 20$ fs. The question at this point is why transient B appears as a distinct feature of the E-AcAc dynamics, although E-AcAc does not switch from one electronic state to another.

Before answering this question we must recall an analysis of Fuss and co-workers.[23] When a neutral system evolves on a potential energy surface, going, for instance, from the Franck−Condon region of excitation to the equilibrium geometry of the surface, the system loses potential energy, which is converted as vibrational energy. A direct vertical ionization by the probe laser preserves this vibrational energy, which is transported into the ion. The latter may subsequently fragment. Accordingly, observing a fragment ion reveals that enough electronic energy has been converted as vibrational energy to overcome the fragmentation barrier of the ion. In other words, observing a fragment ion gives access to the time scale for the energy redistribution to be advanced enough for inducing the ion fragmentation.

(28) Lochbrunner, S.; Schultz, T.; Schmitt, M.; Shaffer, J. P.; Zgierski, M. Z.; Stolow, A. *J. Chem. Phys.* **2001**, *114*, 2519−2522.

We now return to discussing the origin of transient B.

Transient B is best observed when considering the fragment ions at masses 85 and 43 amu under the mild focusing regime of the probe laser. In this experiment, transient A is not observed ($\sigma_A < 0.01$ in Table 2) and transient B is the best observed transient ($\sigma_B = 0.69$ and 0.76 when observing masses 85 and 43 amu, respectively). From the analysis above, we infer that that the induction time of $\tau_A = 70 \pm 10$ fs to populate transient B from transient A would be the time to bring enough vibrational energy into the excited neutral molecule to stimulate the ion dissociation upon ionization.

The energy transfer that accompanies the switch from transient A to transient B is likely to broaden the absorption bands of the excited molecule. Following an argument that has already been used, this enhances the probability for multiphotonic detection. A striking point revealed under the soft focusing regime of the probe laser substantiates this expectation: the top panel of Figure 6 reports electron spectra recorded at two delays with normalization on the electrons of low energy. The electrons of 0.34, 0.65, 0.95, and 1.19 eV are present only as an unstructured tail at short delays (full triangles) whereas they are fully developed at longer times (open triangles). Electrons of such large energy are necessarily produced by a four-photon ionization process, although the soft focusing regime stimulates the detection by a three-photon process, which produces electrons of low energy. The enhanced efficiency of the four-photon ionization process in the range of delays 120−400 fs is an indirect indication of energy redistribution.

The question at this point is why transient B decays to transient C in 100 ± 20 fs and appears as a distinct dynamical feature compared with transient C. Indeed, the fragmentation that is subsequent to the ionization should be comparable in transients B and C, which both have experienced the energy redistribution within the S_2 state. A possible explanation is that the wavepacket describing the movement on the S_2 surface is still fairly localized (has not lost fully its coherence) and transient B corresponds to a region where an accidental resonance exists with an upper Rydberg surface, which enhances the efficiency of the multiphoton ionization. Of course, such an effect must be especially apparent under the soft focusing regime of the probe laser. Inspection of Table 2 confirms this expectation: the difference between σ_B and σ_C is much larger for the experiment performed under the soft focusing regime than for that under the mild focusing regime.

5.6. Toward Observing the Energy Redistribution within the S_2 State. The above discussion suggests that the dynamics from transient A to C corresponds to a relaxation of the initial excess energy within the potential well of the S_2 state. We have also said that the enolic H atom is destabilized by the electronic excitation, and the picture that emerges from the above discussion is the following. Upon excitation of E-AcAc to the S_2 state, the enolic H atom starts movements along the O−H stretch. This initiates an intramolecular vibrational relaxation (IVR) toward the most coupled modes, the C−O−H bending and C=C−O−H torsion modes. The coupling to the other modes follows, the molecules still being in the S_2 state.

The O−H stretch vibrational period is ca. 10 fs, and the corresponding movement is not time-resolved with the time resolution of the present experiment, 80 fs. Probing this vibrational mode thus appears as probing the population of a series of vibrational levels. In contrast, the vibrational movement along the other deformation modes is much slower and a deformation along these modes is time-resolved in the present experiment. Hence, a movement along these modes is described by a vibrational wavepacket. Upon excitation by the pump laser, it is localized in the Franck−Condon region of the excitation. During the time $\tau_A + \tau_B + \tau_C$, it progressively loses its coherence within the multidimensional S_2 potential surface, τ_C being the time scale for the wavepacket to transfer to the S_1 state.

The progressive energy relaxation of the O−H stretch and the loss of coherence of the vibrational wavepacket should show up in the dependence of the electron spectrum as a function of the pump/probe delay. The resonances mentioned in the previous section certainly obscure this information since the resonance-enhanced ionization depends on the location and spreading of the wavepacket. The mild focusing regime is less sensitive to the resonance effects than the soft one because intermediate steps are saturated. Hence, electron spectra taken under the mild focusing regime are now considered. They are shown in the bottom panel of Figure 6. The important observation is that the features at 0.65, 0.95, and 1.19 eV are partially lost and probably broaden also when the delay increases from the range of 0−70 fs (full triangles) to 1200−2000 fs (full circles). Also, the broad contribution at 0.34 eV becomes a bit broader without changing intensity very much.

It is interesting to note that the bands at 0.34, 0.65, 0.95, and 1.19 eV can be assigned to a vibrational progression of the S_2 state that is energy-resolved. It corresponds to a vibrational constant of $\omega_e = 2860 \pm 80$ cm^{-1} and an anharmonicity parameter $\omega_e x_e = 140 \pm 20$ cm^{-1}. Accordingly, the 0.34, 0.65, 0.95, and 1.19 eV electron energies could be the excess energies above ionization when ionizing the $v = 0, 1, 2, 3$ levels of vibrational progression in the S_2 state.

The ν_{OH} frequency of ground-state E-AcAc is calculated at 3022.9 cm^{-1}.[29] The O−H bond is stretched in S_2 since the H atom is halfway between the two O atoms. Hence, a lower ν_{OH} frequency is expected in S_2. The vibrational progression with $\omega_e = 2860 \pm 80$ cm^{-1} might thus be assigned to the ν_{OH} mode in S_2, consistently with the above expectation that this mode is not time-resolved. Accordingly, the features at 0.65, 0.95, and 1.19 eV that weaken when increasing the pump−probe delay may thus reflect the decreasing population of the $v = 1, 2, 3$ levels of this progression. Because of the energy conservation within the isolated molecule, the population that is transferred to the $v = 0$ level of the O−H stretch also corresponds to a population scattered over the numerous vibrational modes of E-AcAc. The result might be a broadening of the 0.34 eV peak as observed experimentally.

Large uncertainties prevail on the latter assignment, especially because it implicitly assumes that the H atom is almost free in the ion when the ionization proceeds from the S_2 state. This results in a ν_{OH} stretch frequency that is close to zero. Work beyond the scope of the present investigation must be done to ascertain this hypothesis. It goes through ab initio calculations of the S_2 and ionic surfaces, along several deformation modes of the molecule. Much more challenging, extensive predictions of the time-dependent electron spectrum would also be helpful.

(29) Trivella, A.; Roubin, P.; Theule, P.; Rajzmann, M.; Coussan, S.; Manca, C. *J. Phys. Chem. A* **2007**, *111*, 3074−3081.

Nevertheless, we consider the results discussed in Figure 6 as potentially important since they bring back interest in the IVR process in excited states.[30-35] The present work focuses on the population decay of a specific vibrational mode and hence goes beyond the picture of a purely statistical regime of vibrational relaxation.

6. Conclusion

The dynamics of the enolic form of acetylacetone (E-AcAc) was explored using a femtochemistry technique. A pump laser tuned at 266 nm was used to excite E-AcAc in its first bright state, S_2, which has $\pi\pi^*$ character. The evolution of E-AcAc on the $S_2(\pi\pi^*)$ and $S_1(n\pi^*)$ surfaces was probed by multiphoton ionization at 800 nm. Molecular ions at 100 amu, fragment ions at 85 and 43 amu, and electrons were detected. Their observation opens several windows on the full dynamics that was followed for 80 ps after the pump pulse. Important steps have been identified along this dynamics process. First, the departure from the Franck−Condon region is found in the time frame of 70 ± 10 fs. The initial deformation is likely the H-atom transfer from one oxygen atom to the other, but more complex deformations are certainly involved in this initial step. Then the system moves to a region of important coupling between the $S_2(\pi\pi^*)$ and $S_1(n\pi^*)$ surfaces, the full transfer of the wavepacket from one surface to the other taking 1.4 ± 0.2 ps. The dynamics after the transfer to the S_1 surface was followed for 80 ps in the present work. It appears as a slow decay, which is consistent with the time scale of 247 ± 34 ps found by Zewail and co-workers for the decay of this state toward triplet states of E-AcAc.[8] Between the departure of the wavepacket from the Franck−Condon region in the S_2 state and its full transfer to the S_1 state, an IVR is at play that transfers excess energy along the enolic group O−H to the other modes of the molecule. There are clues from the deformations of the electron spectrum as a function of the delay between the pump and the probe lasers that the IVR process is observed directly.

The picture above is likely to be fairly general and should apply to the enolic form of many β-diketones. In particular it is consistent with the work of Stolow and co-workers on larger enolic β-diketones where the C=C double bond is conjugated with a phenyl group.[28]

Several points of the above scenario need to be examined further. First, the nature of the coupling between the $S_2(\pi\pi^*)$ and $S_1(n\pi^*)$ surfaces must be identified. It is likely a conical intersection as is the case in malonaldehyde, but the available calculations on E-AcAc do not yet provide this information. Second, the decay of S_1 is believed to involve an intersystem crossing with triplet states. The calculations by Chen et al. suggest that the picture is correct.[13] However the calculations of Martinez and Coe on malonaldehyde suggest a more complex dynamics with a conical intersection between three singlet surfaces.[17] Hence, it would be useful to detect excited E-AcAc after its departure from the S_1 state. Unfortunately, this was not possible with the laser wavelengths available at the present laser facility. Finally and most importantly, the direct observation of the IVR process has yet to be confirmed by very high-level ab initio calculations of the S_2 and ionic surfaces, along several deformation modes of the molecule, coupled to dynamical calculations, in order to predict the time-dependent shape of the photoelectron spectrum.

(30) Smith, J. M.; Zhang, X.; Knee, J. L. *J. Chem. Phys.* **1993**, *99*, 2550−2559.
(31) Zhang, X.; Smith, J. M.; Knee, J. L. *J. Chem. Phys.* **1994**, *100*, 2429−2436.
(32) Hineman, M. F.; Bernstein, E. R.; Kelley, D. F. *J. Chem. Phys.* **1993**, *98*, 2516−2523.
(33) Bingemann, D.; Gorman, M. P.; King, A. M.; Crim, F. F. *J. Chem. Phys.* **1997**, *107*, 661−664.
(34) Hammond, C. J.; Ayles, V. L.; Bergeron, D. E.; Reid, K. L.; Wright, T. G. *J. Chem. Phys.* **2006**, *125*, 124308.
(35) Zuo, P.; Sutresno, A.; Li, C.; Koyama, Y.; Nagae, H. *Chem. Phys. Lett.* **2007**, *440*, 360−366.